Ferrielectricity in the Archetypal Antiferroelectric, $PbZrO_3$

*Yulian Yao Aaron Naden Mengkun Tian Sergey Lisenkov Zachary Beller Amit Kumar Josh Kacher Inna Ponomareva Nazanin Bassiri-Gharb**

Dr. Yulian Yao, Prof. Josh Kacher, Prof. Nazanin Bassiri-Gharb*

Affiliation: School of Materials Science and Engineering, Georgia Institute of Technology, Atlanta, Georgia, USA

*Email Address: nazanin.bassirigharb@me.gatech.edu

Dr. Aaron Naden, Prof. Amit Kumar

Centre for Nanostructured Media, School of Mathematics and Physics, Queen's University Belfast, Belfast, United Kingdom

Dr. Aaron Naden

School of Chemistry, University of St Andrews, St Andrews, United Kingdom

Dr. Mengkun Tian

Materials Characterization Facility, Institute for Electronics and Nanotechnology, Georgia Institute of Technology, Atlanta, USA

Prof. Sergey Lisenkov, Prof. Inna Ponomareva

Department of Physics, University of South Florida, Tampa, Florida, USA

Zachary Beller, Prof. Nazanin Bassiri-Gharb

G.W. Woodruff School of Mechanical Engineering, Georgia Institute of Technology, Atlanta, Georgia, USA

Keywords: *antiferroelectric, ferrielectric, $PbZrO_3$, thin film, anisotropy*

Antiferroelectric materials, where the transition between antipolar and polar phase is controlled by external electric fields, offer exceptional energy storage capacity with high efficiencies, giant electrocaloric effect, and superb electromechanical response. $PbZrO_3$ is the first discovered and the archetypal antiferroelectric material. Nonetheless, substantial challenges in processing phase pure $PbZrO_3$ have limited studies of the undoped composition, hindering understanding of the phase transitions in this material or unraveling the controversial origins of a low-field ferroelectric phase observed in lead zirconate thin films. Leveraging highly oriented $PbZrO_3$ thin films, a room temperature ferrielectric phase is observed in absence of external electric fields, with modulations of amplitude and direction of the spontaneous polarization and large anisotropy for critical electric fields required for phase transition. The ferrielectric state observations are qualitatively consistent with theoretical predictions, and correlate with very high dielectric

This article has been accepted for publication and undergone full peer review but has not been through the copyediting, typesetting, pagination and proofreading process, which may lead to differences between this version and the Version of Record. Please cite this article as doi: 10.1002/adma.202206541

tunability, and ultra-high strains (up to 1.1%). This work suggests a need for re-evaluation of the fundamental science of antiferroelectricity in this archetypal material.

Antiferroelectric materials offer superior energy storage properties, extremely large electromechanical response (and concomitant large displacement and forces), in addition to co-presence of positive and negative electrocaloric effects [1, 2]. These enhanced properties are enabled by the characteristic antipolar to polar (AP→P) phase transition, which translates into a functional linear dielectric to ferroelectric change. The original theory of antiferroelectricity was developed by Kittel 1951, in parallel with antiferromagnetism [3], and reported experimentally the same year in $PbZrO_3$[4]. Since its discovery, lead zirconate has been considered as the archetypal antiferroelectric oxide, and is the basis for many antiferroelectric ceramics, in addition to being the end member of one of the most widespread piezoelectric ceramics, lead zirconate titanate (PZT). In $PbZrO_3$, in absence of an applied electric field, each unit cell is polar (space group Pbam). However, an antiparallel arrangement of dipoles along $[100]_O$ results in a net zero (macroscopic) polarization. Beyond a critical field, E_f , the dipoles align, resulting in the creation of a polar, ferroelectric phase. By reducing the electric field, the material hysteretically returns to the antipolar phase at an electric field, E_a, smaller than E_f.

Most recently, with increasing studies on antiferroelectric materials, a low-field ferroelectric phase and incommensurate modulations have been reported in lead zirconate-based antiferroelectric materials[5, 6, 7, 8]. Similarly, recent theoretical simulations have suggested a complex, 80-atoms unit cell in $PbZrO_3$, doubling the c-axis of the *Pbam* structure[9], as well as a possible stable ferrielectric state, with lower energy than the antiferroelectric one at room temperature[10]. Lastly, previous computational and experimental studies have reported that in ultra-thin films or nanostructure form, $PbZrO_3$ can exhibit pure ferroelectric behavior[11, 12, 13]. This body of experimental and theoretical work indicates that the arrangement of dipoles in $PbZrO_3$ might strongly deviate from the "ideal" double antiparallel configuration, and yet a dearth of experimental reports on this prototypical antiferroelectric endures in the literature. The persistence of contradictory literature reports and a lack of a clear, unified, understanding of the observed functionalities have been a direct result of challenges in processing undoped, phase pure $PbZrO_3$ (plagued with extremely low breakdown strength) and limited systematic orientation studies[7, 14].

This work leverages $PbZrO_3$ thin films – processed via low-cost chemical solution deposition on platinized Si substrates – to probe the anisotropic dielectric and electromechanical response associated with the electric field-induced phase transitions, and ultimately the origin of the hitherto controversial low-

field ferroelectric phase previously reported in these films. We map local polarization via high-resolution scanning transmission electron microscopy (HRSTEM) and find anisotropic modulations of amplitude and direction of the spontaneous polarization across adjacent unit cells. Specifically, polarization modulations in direction and amplitude are observed in {120} and {100} planes, an experimental support to the recent proposal of stable ferrielectricity in $PbZrO_3$, based on first-principles calculations[10].

$PbZrO_3$ thin films are processed by chemical solution processing on platinized Si substrates and have an orthorhombic, perovskite phase with strong preferential orientation **Figure 1**. X-ray diffraction (XRD) indicates that the films are highly 001- and 042-oriented with Lotgering factors (LF) of 97% and 99%, respectively[15]. The estimated d-spacings are $d_{002} = 4.11$ Å and $d_{042} = 2.39$ Å, consistent with single crystal values ($d_{002} = 4.110$ Å and $d_{042} = 2.373$ Å)[16]. An evaluation of the same through HAADF STEM (Figure 1d-e), indicates that the d-spacings are $d_{002} = 4.13\pm0.004$ Å and $d_{042} = 2.37\pm0.01$ Å for the 001- and 042-oriented films, respectively. These results suggest that the 042-oriented sample might be subject to small residual stresses within the film. However, we note that for the same sample, $d_{044} = 1.69\pm0.01$ Å, still consistent with the 1.69 Å reported for the single crystal. Hence, any eventual residual stresses even within the 042-oriented samples are anisotropic. The electron backscatter diffraction (EBSD) mapping and the derived inverse pole figure (IPF), as shown in Figure 1b-c, further confirm that the $PbZrO_3$ films are highly oriented.

The preferred orientation correlates with a difference in grain size, with the 001-oriented film having a mean grain size of ∼100 nm, and the 042-oriented film having a mean grain size of ∼144 nm. The grain boundary misorientation distribution for both films spans a wide range and no evident preferred rotation values **Figure S1**. Atomic resolution high-angle annular dark-field (HAADF) STEM and corresponding fast Fourier transform (FFT) images of the cross-sectional areas of 042- and 001-oriented films in Figure 1d reveal the overall arrangement of atoms consistent with a *Pbam* structure previously reported for this material, and the FFT images match well with diffraction patterns of single crystal $PbZrO_3$ with zone axis of $[\bar{1}00]$ and $[\bar{2}10]$, respectively **Figure S2**.

The macroscopic functional response of both sets of films is consistent with the expected antiferroelectric response, **Figure 2**. The electric field induced polarization (*P-E*) measurements show double hysteresis loops, and the switching currents show four distinct peaks, all characteristic of antiferroelectric materials. However, the electric fields for polar and antipolar transition are strongly orientation dependent. The 042-oriented $PbZrO_3$ has an E_f of $\sim 350kV/cm$ and square *P-E* loops Figure 2a, upper left. The switching current (*I-E*) curves Figure 2a, bottom left show sharp, narrow peaks, corresponding to

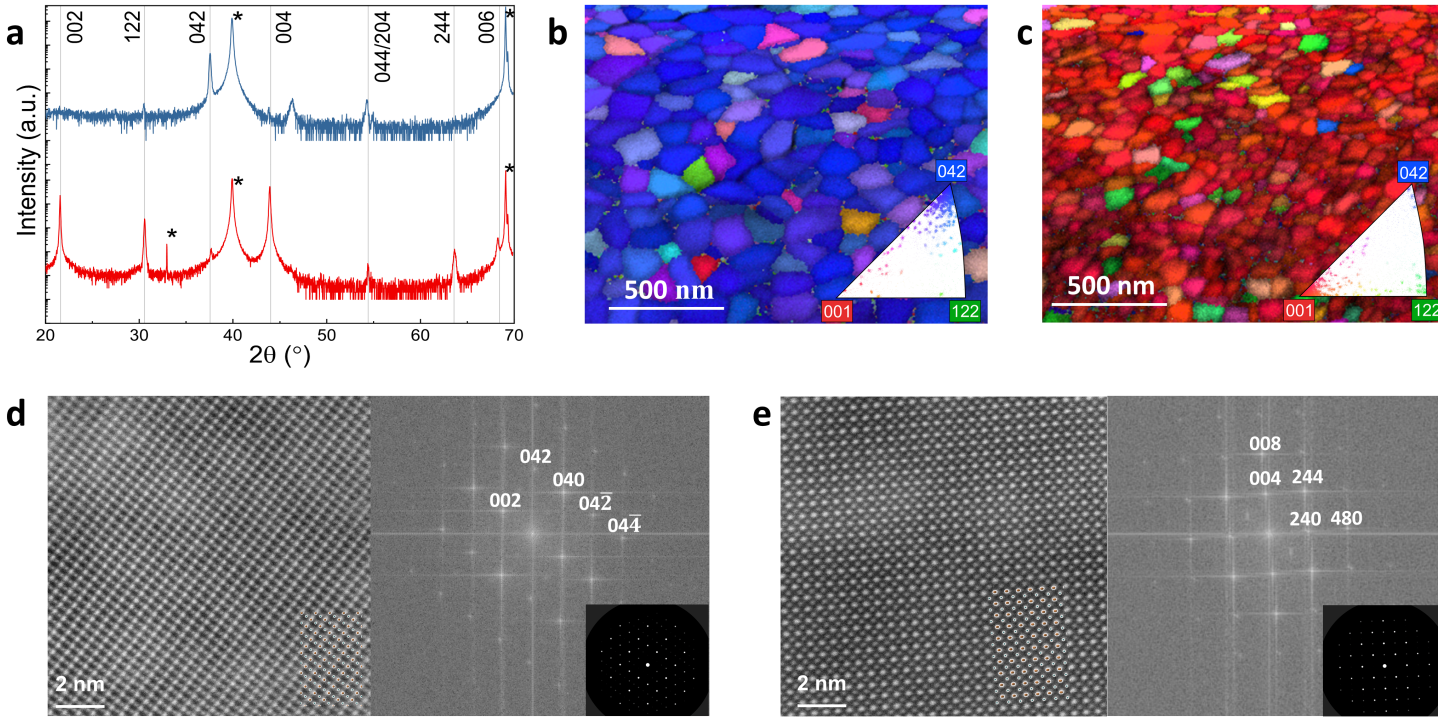

Figure 1: (Micro-)Structure of $PbZrO_3$ thin films. (a) X-ray diffraction (XRD) patterns plotted with intensity in logarithmic scale. The peaks labelled with star are from the platinized Si substrate. (b, c) Electron backscatter diffraction (EBSD) orientation maps and derived inverse pole figures (insets) of (b) highly 042- and (c) 001-oriented $PbZrO_3$ thin films' surface. Atomic resolution (HAADF) STEM images with overlapping theoretical arrangements of Pb^{2+} and Zr^{4+} ions (bottom right corner), corresponding fast Fourier transformation (FFT) images, and theoretical single crystal diffraction patterns (insets) of (d) 042- and (e) 001-oriented $PbZrO_3$ thin films. The Pb atom columns appear brighter and larger, with the darker and smaller Zr atom columns forming a pseudo-cubic lattice. The streaking in FFT images is an artifact due to discontinuity of intensities at image edge.

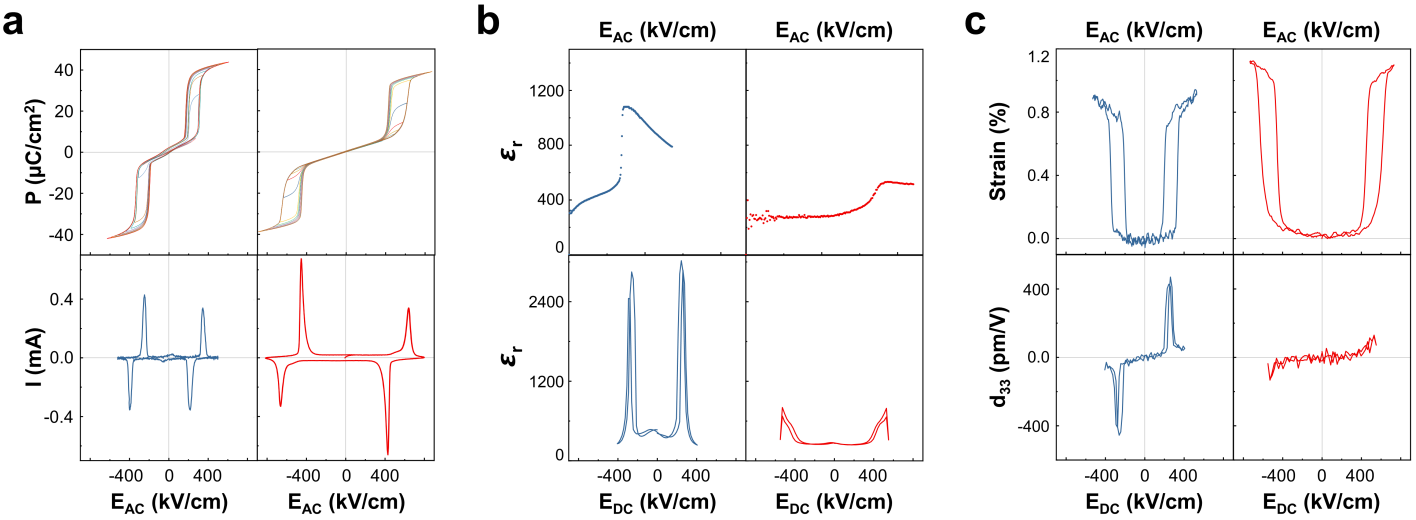

Figure 2: Anisotropic dielectric and electromechanical properties of $PbZrO_3$ thin films. (a) Polarization (P) and switching current (I) as a function of applied AC electric fields (E_{AC}); (b) dielectric permittivity (ϵ_r) as a function of AC (top) and DC electric fields, E_{DC} (bottom), representing dielectric nonlinearity and dielectric tunability in the films, respectively. (c) electromechanical response as strain, S (top), and effective longitudinal piezoelectric coefficient, $d_{33,f}$ (bottom), as a function of E_{AC} and E_{DC}, respectively. The response of 042- and 001-oriented films is shown in blue (left-side) and red (right-side), respectively.

a narrow window of applied electric field for the $AP \iff P$ phase transitions. The highly 001-oriented film has much higher E_f (~620 kV/cm) and a more diffuse $AP \rightarrow P$ phase transition (Figure 2a, bottom right). The anisotropy in the E_f is consistent with first-principles computations for the polar/antipolar phases' coexistence field, E_{coex}, in bulk $PbZrO_3$ (**Figures S3 and S4**). The diffuse and shallow forward transition in 001-oriented films could be due to a very small number of 122-oriented grains in the 001-oriented samples(Figure 1a).

Consistent with the polarization switching anisotropy, the electric field dependence of the dielectric permittivity is also dramatically orientation dependent. With relatively small forward (E_f) and reverse (E_a) transition fields, 042-oriented films show ultra-high dielectric tunability of ~92% within a 250 kV/cm electric field change (Figure 2b, bottom left). In comparison, the 001-oriented films break down before the full polar transition is achieved under applied DC electric fields. Despite this shortcoming, the 001-oriented films show a relatively large dielectric tunability of 70% with an incomplete the AP → P phase transition (Figure 2b, bottom right). The anisotropic phase transitions translate also in different energy storage performance for the 001- and 042-oriented films (**Figure S5**). The 001-oriented films offer a higher energy storage density (up to 16 J/cm^3) with storage efficiency of over 75% compared to the 042-oriented films, that exhibit approximately half of the 001 films' maximum energy density and lower storage efficiency.

Both films offer very large strains at phase transition, in excess of 0.94% for 042-oriented samples

and ∼1.14% for 001-oriented samples (Figure 2b). The effective longitudinal piezoelectric coefficient, $d_{33,f}$, is also measured as a function of applied DC electric fields. 042-oriented films show an ultra-high $d_{33,f}$ of slightly over 450 pm/V at phase transition, while 001-oriented $PbZrO_3$ films break down before the AP → P phase transition is completed, consistent with the dielectric tunability and switching current experiments.

Intriguingly, a low-field ferroelectric phase is observed in the 042-oriented films in all functional characterizations. This weak ferroelectric phase manifests as a small loop in *P-E* measurements at low fields - and a remanent polarization of ∼2.3 $\mu C/cm^2$ - and two additional peaks at ∼30-50 kV/cm in the *I-E*$_{AC}$ and dielectric tunability curves. Additionally, the dielectric response of the 042-oriented films is strongly nonlinear at intermediate AC electric fields (Figure 2b, top left), increasing continuously with increasing applied electric fields (before the polar transition). Dielectric nonlinearity is a signature of extrinsic contributions to the dielectric permittivity[17], often associated with the motion and vibration of domain walls and phase boundaries in ferroelectric materials. Conversely, the 001-oriented films do not show any remanent polarization distinguishable from the background, no additional peaks are observed in the *I-E*$_{AC}$ curves corresponding to eventual ferroelectric polarization switching, and a field-independent dielectric permittivity is observed for these films up to ∼300 kV/cm, consistent with absence of ferroelectricity.

The appearance of a ferroelectric phase in $PbZrO_3$ thin films has been ascribed to many different factors. For example, it has been suggested that the ferroelectric phase arises due to the presence of uncompensated charges at the film surface and/or at the interface with the bottom electrode[18, 19]. However, in our case, the ferroelectric contribution remained unchanged in 540 nm-thick, 042-oriented $PbZrO_3$ films (**Figure S6**), ruling out the exclusive effects of free surfaces and buried interfaces. Another theory for stabilization of a ferroelectric phase in $PbZrO_3$ thin films has been offered based on Pb over-stoichiometry and formation of Pb antisite defects[20]. However, no obvious Pb antisite defects were observed in any samples in this work. Specifically, no obvious antisite defects were observed in the HAADF images (Figure 1), and the Pb:Zr molar ratio in both the 042- and 001-oriented films is close to 1:1 (**Figure S7**) with no apparent elemental segregation at grain boundaries. Indeed, the Pb:Zr ratio in the 042-films, where the room temperature low-field ferroelectric phase is observed, is slightly inferior to that of the 001-oriented films. Hence, stabilization of a perovskite $PbPbO_3$ phase leading to ferroelectricity at low field is also ruled out.

Alternatively, a high-temperature ferroelectric phase - predicted in $PbZrO_3$ and demonstrated re-

cently with intriguing polarization ordering[8] – could be stabilized through stress in differently oriented films. In our work, this high-temperature ferroelectric phase can be observed in the local maxima in dielectric loss measurements as a function of temperature (**Figure S8**) and increased remanent polarization in temperature-dependent *P-E* loops (**Figure S9**) within a similar temperature range. The transition to this high-temperature ferroelectric phase is observed at ∼240°C and ∼200°C, for 001- and 042-oriented films, respectively. The slight difference in the transition temperature might imply a higher residual tensile stress in 001-oriented films compared to the 042-oriented samples. This observation is consistent with the higher Curie Temperature in the 001-oriented samples compared to the 042-oriented films (Figure S8) as well as the 001-oriented films requiring a higher E_f and E_a at a given temperature than the 042-oriented films (**Figure S10**).

No trace of a ferroelectric phase stable at lower temperatures (down to room temperature) is observed in the 001-oriented films' dielectric response or polarization. However, a separate low-temperature, low-field ferroelectric phase persists in 042-oriented films in the temperature range from 25 to 75°C (Figure S9 and **S11**), expressed as a small loop in the *P-E* curves and a minor peak in the loss tangent curves. A low temperature ferroelectric phase has been also previously reported in literature[14, 21]. However, in such cases, the low-field ferroelectric phase was observed only at substantially lower temperatures. At below ∼200 K a metastable orthorhombic ferroelectric phase was observed upon application of a high enough electric field along the $[210]_O$ of $PbZrO_3$ single crystals, and did not revert to an antipolar phase upon removal of the applied electric field; conversely, upon application of an AC electric field, a stable ferroelectric phase appeared[22]. In our work the low-field ferroelectric phase was reversibly and persistently observed over multiple experiments, irrespective of number of cycles, the applied field's strength, or application of either AC or DC fields. In another work, a phase transition to a stable ferroelectric P-E_{AC} hysteresis loop was observed in 001-oriented films at below 60 K, with a maximum in capacitance and loss tangent as a function of temperature at ∼16 K; but, the authors observed a mixture of antiferroelectric and ferroelectric response in 120-oriented films in the 4.2–400 K temperature range[14]. Thus, consistent with the previous work, the low-temperature, low-field ferroelectric phase observed in the present study is not a result of stabilization through residual stresses from lower or higher temperatures: the room temperature, low-field ferroelectric phase is highly dependent on the films' orientation, regardless of the residual stress states.

Having eliminated the above possible contributors to the room temperature low-field ferroelectric phase, we now look at the anisotropic polarization arrangement in $PbZrO_3$ films. In $PbZrO_3$, the rel-

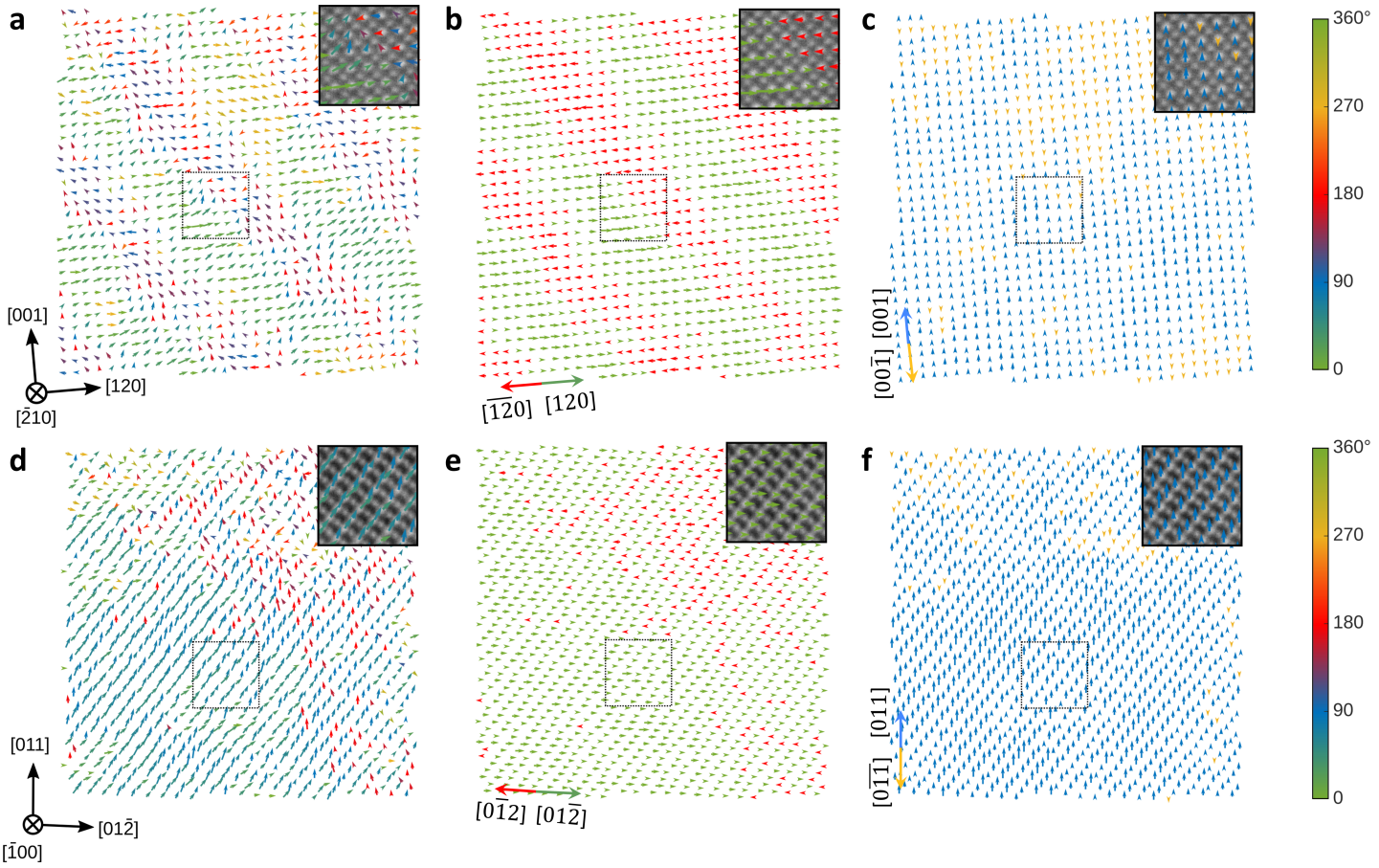

Figure 3: Polarization configurations extracted from Pb ions displacements in 001- and 042-oriented films with enlarged sections of HAADF images underlaid in the upper right hand corner of each plot. (a, d) Displacement of Pb^{2+} ions and their relative components (b, e) in the surface plane and (c, f) along the film surface normal for (a-c) 001-oriented and (d-f) 042-oriented films, respectively. All data are obtained from atomic resolution high-angle annular dark-field (HAADF) images in Figures 1d and 1e. The color scale in (c) applies to panels (a-c) and uses [120] as reference (0°) and the color scale in (f) applies to panels (d-f) and uses $[04\bar{4}]$ as reference (0°). The rotation of the mapping relative to film orientation is a result of a slight misorientation of scan angle during STEM imaging to avoid imaging artefacts. Additional local polarization maps of the 001- and 042-oriented films are available in **Figures S12-S15**.

ative displacement of Pb^{2+} ions against the center of oxygen octahedra are found to have much larger displacement than Zr^{4+} ions[23], and ultimately, Pb^{2+} ions are the main contributors to the local polarization [16, 24, 25]. A comparison of local Pb displacement in 001- and 042-oriented films based on HRSTEM images is shown in **Figure 3**. According to the classical interpretation of antiferroelectricity in $PbZrO_3$, Pb^{2+} ions are expected to show double antiparallel displacement along the $[100]_O$ direction. Nonetheless, in the present study Pb displacement is found to consistently show modulations in both direction and amplitude in both films, including in planes perpendicular to $[100]_O$ (Figure 3).

Specifically, 001-oriented films show modulations of polarization across the film thickness, with a banding thickness of ∼4−6 atoms (Figure 3a and 3b). The projections of Pb displacement along in-plane (Figure 3b) and out-of-plane directions (Figure 3c) show that the banding is mostly a result of polarization direction changes in the in-plane (with respect to film's surface) direction. Additionally, while the

average number of dipoles in each band is similar, the Pb displacement along $[120]_O$ shows larger magnitudes (∼0.09 Å) than the opposite direction (∼0.06 Å), as shown in Figure 3b, suggesting a non-zero macroscopic remanent, spontaneous polarization component along this direction. Pb displacement is also calculated in the mapped area in Figure 3a. Along $[120]_O$, the averaged Pb displacement for each line of atoms is calculated to be ∼1 Å, which is close to the averaged Pb displacement along $[001]_O$ direction (~ -1.1 Å), suggesting similar remanent, spontaneous polarization along $[120]_O$ and $[001]_O$ directions. The polarization in out-of-plane direction (with respect to the film's surface) is shown in Figure 3c: the volumes of material with opposite relative polarization are intermixed, without a clear banding of similarly oriented dipoles. Hence, macroscopically this polarization contribution is expected to be small, consistent with the insignificant remanent polarization measured in the 001-oriented films.

Compared to the 001-oriented films, 042-oriented samples offer a very different polarization configuration. As shown in Figure 3d, while the displacements of the Pb atoms show both amplitude and direction modulations, no polarization banding is observed either in the in-plane or out-of-plane directions (with respect to the film surface). Absence of dipole bands might be due to a more homogeneous polarization throughout the film or bands wider than the mapped area, consistent with previous reports of $PbZrO_3$ bulk ceramics, with approximately 500 nm wide domains[26]. Pb displacement along $[011]_O$ and $[01\bar{2}]_O$ in Figure 3d is also calculated. Along $[01\bar{2}]_O$, the averaged Pb displacement for each line of atoms is ∼1.7 Å, while along $[011]_O$, the averaged Pb displacement is ~ -2.9Å. The substantially larger out-of-plane Pb displacement compared to 001-oriented films is consistent with our observations of a room temperature ferroelectric phase in the 042-oriented films, resulting in an observable remanent polarization at zero field. However, Pb displacement in 100 planes (of 042-oriented films) is in contradiction to the accepted antiferroelectric structure of $PbZrO_3$, which requires zero Pb displacement along directions perpendicular to [100]. Additional polarization maps obtained throughout the films' thickness are shown in Supplementary Information with very similar observations of Pb displacement throughout the films' thickness **Figures S12-S15**.

Our results are indeed substantially closer to incommensurate modulations – i.e. a structural ordering with non-integral modulation vector – previously reported in $Pb_{0.98}Nb_{0.02}(Zr_{0.35}Sn_{0.25}Ti_{0.40})O_3$ bulk ceramics and $(Pb_{0.97},La_{0.02})(Zr_{0.95},Ti_{0.05})O_3$ thin films at room temperature, due to frustrated competition between long-range ferroelectric and short-range antiferroelectric phases [5, 27, 28]. In such cases, uncompensated incommensurate modulations translate into a net remanent polarization at zero electric field. Furthermore, uncompensated modulations of polarization at the nanoscale can be also considered

as ferrielectricity, as recently reported in bulk $Pb_{0.97}La_{0.02}(Zr_{0.50}Sn_xTi_{0.50-x})$ (x = 0.50, 0.45, 0.375) ceramics [6]. First reported in 1960 [29], ferrielectricity is by default strongly anisotropic and can translate into ferroelectric response along specific crystallographic directions and antiferroelectric properties along others. While, reports on ferrielectric crystals (except in polymeric materials) have been particularly rare [6, 30], recent theoretical studies have indicated the possibility of a ferrielectric phase with higher stability than the antiferroelectric phase in room temperature $PbZrO_3$[10]. To explore whether this proposed ferrielectric phase could be a possible candidate for our low-field ferroelectric phase, we computed its polarization and found that it would contribute by 0.0 and 12.5 $\mu C/cm^2$ along the direction of measurement for 001 and 042 films, respectively. Therefore, although larger than the experimental observations, the previously theoretical ferrielectric phase is in excellent qualitative agreement with our anisotropic experimental observations.

Based on the above and the fact that the modulation of polarization is both orientation dependent and incommensurate, we argue that the $PbZrO_3$ films should be considered in a ferrielectric phase at room temperature and in absence of strong external electric fields. We note that the macroscopic and averaged functional and structural characteristics of these samples (e.g., double P-E_{AC} and bipolar strain hysteresis loops, quadruple transitions in the I-E_{AC} curves shown in Figure 2), are consistent with those considered as signatures of an antiferroelectric material. However, it is the microscopic features that depart substantially from those of an antiferroelectric structure. The fact that the archetypal antiferroelectric $PbZrO_3$ material does not indeed follow the traditional theory of antiferroelectricity, but rather offers features more consistent with ferrielectricity is worth substantially greater consideration by the scientific community. We hypothesize that ferrielectricity might emerge in other antiferroelectric compositions, in proximity of the stability of the ferroelectric phase, as a transitional dipole arrangement, and hence, might be further stabilized in thinner films.

Lastly, we note that the amplitude and orientation modulation of polarization in these films offers substantial similarities to relaxor-ferroelectric materials. In relaxor-ferroelectrics, the “malleability" associated with the large underlying chemical and structural heterogeneities have been long considered as a major contributor to their very large dielectric and electromechanical response. Indeed, the developed strain and piezoelectric coefficient ($d_{33,f}$) of the highly oriented, phase pure, undoped $PbZrO_3$ thin films in this work are substantially superior to many $PbZrO_3$-based antiferroelectric, PZT ferroelectric, and relaxor-ferroelectric (1-x)[$Pb(Mg_{1/3}Nb_{2/3})O_3$]-x[$PbTiO_3$] (PMN-PT) films reported in literature (**Figure 4**). The herein reported ferrielectric phase offers not only a “malleable" polarization, but also substantial

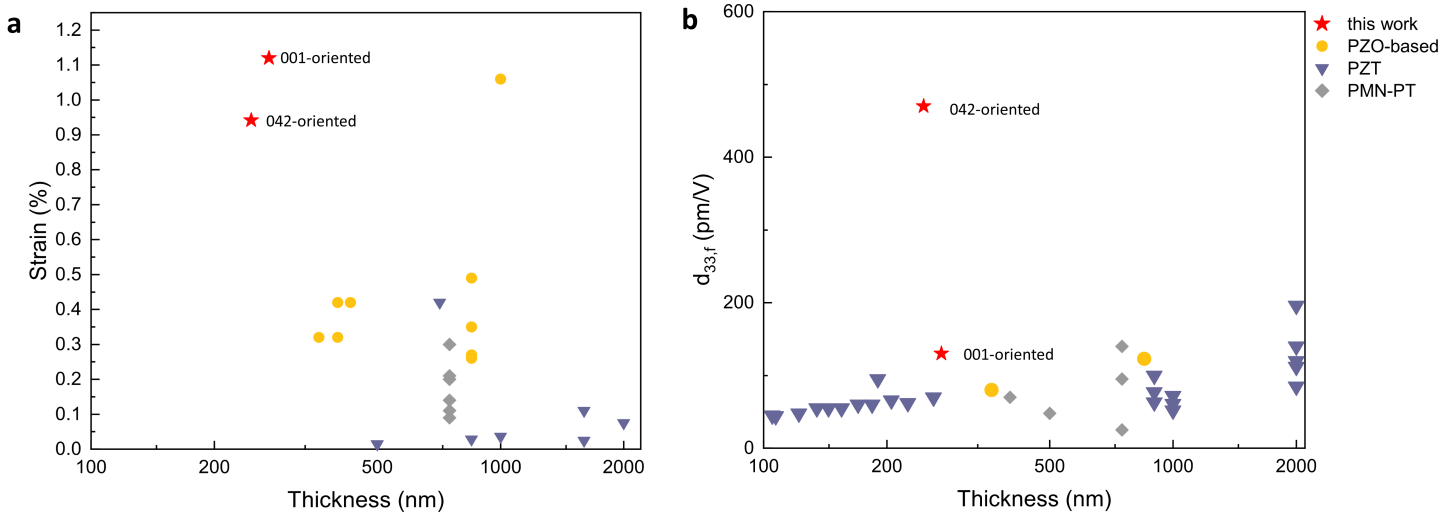

Figure 4: Comparison of electromechanical properties of $PbZrO_3$ films and other antiferroelectric and ferroelectric materials. (a) maximum strain and (b) piezoelectric coefficient ($d_{33,f}$) of $PbZrO_3$ thin films in this work, with other antiferroelectric PZO-based [33, 34, 35], ferroelectric PZT[36, 37, 38, 39, 40, 41, 42], and relaxor-ferroelectric PMN-PT[42, 43, 44, 45] thin films reported in literature.

access to polarization "design" through the strong orientation dependence of the properties. It is noteworthy that compared to the above ferroelectric-based compositions, antiferroelectric-like materials have lower dielectric loss, do not require pre-poling, and do not suffer from thermal, electrical or stress depoling that largely limit the functional range of ferroelectric materials in electromechanical applications [31, 32]. Additionally, the very high electromechanical response in our $PbZrO_3$ thin films is obtained in samples processed via simple, low-cost chemical solution deposition rather than epitaxially grown on expensive substrates by complex tools requiring resource-intensive (ultra)high vacuum. The superior electromechanical response and simple, low-cost preparation method make these $PbZrO_3$ thin films a competitive and promising material for applications in nano-electromechanical devices. It is similarly possible that the malleable state of the polarization would offer, along specific directions, easily tunable polarization, enabling memristive devices.

Experimental Section

Sample Preparation: The $PbZrO_3$ precursor solution were prepared by a 2-methoxyethanol (2MOE)-based route with 70% excess Pb, described elsewhere[46]. Film orientation was controlled through the use of a 0.08 M PbO solution (2MOE as solvent) seed layer to achieve 001-oriented films, 042-oriented films were expected in the case that a seed layer was not used. $PbZrO_3$ thin films were prepared by spin coating onto platinized Si substrates (80 nm Pt/20 nm $Ti/SiO_2/Si$). The films were spin coated at 3000 rpm for 30 seconds onto the substrates and pyrolyzed at 400 °C for 1 minute after each coating. The films were crystallized, every two deposition and pyrolysis, in a rapid thermal annealer (RTA) or an oven

at 725 °C for 1 minute. For the films with PbO seed layer, the PbO solution was spun coated at 3000 rpm for 30 seconds and pyrolyzed at 400 °C for 1 minute. The PbO layer was also crystallized at 700 °C for 1 minute before the deposition of $PbZrO_3$ layers.

X-ray Diffraction: XRD scans were performed with a Malvern PANalytical Alpha-1, with monochromated incident Cu-Kα X-ray of wavelength 1.540598 Å. The operating power was set at 45 kV and 40 mA for the Cu X-ray source. 2θ scans from 20° to 70° with step size of 0.02° and scan rate of 10 seconds/° were performed. The optics used for the scans were 0.04 radian Soller slit for both incident and receiving beams, 10 mm mask for incident beam, 1° anti-scatter slit, and 5.5 mm anti-scatter slit for the diffracted beam. The $PbZrO_3$ films were leveled with the sample holder and the obtained diffraction data were further aligned with 400-Si peak at 69.15°.

Electron Microscopy: EBSD and (S)TEM cross-section preparation were performed on an FEI Scios DualBeam FIB-SEM system equipped with an EDAX Hikari XP EBSD system. EBSD was performed at an accelerating voltage of 20 kV, nominal probe current of 1.6 nA and with $SrTiO_3$ as the reference perovskite solution. Orientation maps and grain size and grain boundary misorientation angle distribution plots were generated using the EDAX software package OIM Analysis. FIB milling was performed at accelerating voltages of 30, 16, 8, 5 and 2 kV. (S)TEM was performed on a probe-corrected FEI Titan Themis operated at 200 kV with a CEOS DCOR spherical aberration corrector. Pairs of HAADF images (inner/outer collection angles of 91 and 200 mrad, respectively) were obtained and corrected for specimen drift using the MATLAB procedure detailed elsewhere[47]. Atomap[48] was used to extract the Pb and Zr atom positions by Gaussian fitting to the drift-corrected data. Theoretical atom arrangements and diffraction patterns used for reference are drawn based on lattice parameters from powder diffraction file (PDF) with reference number 04-015-9392[49].

Functional Characterization: Top circular electrodes with diameters of 100 μm, 500 μm, and 1 mm were deposited by sputtering (through a shadow mask) 80 nm of Pt in a Unifilm tool in Ar environment (5 mTorr). All functional characterizations were performed on the electrodes with diameter of 500 μm, unless otherwise specified. The dielectric response of as-prepared $PbZrO_3$ films was measured with an Agilent 4284A Precision LCR-meter (Agilent Technologies, Santa Clara, CA) at 1 kHz and 100 mV. Polarization versus electric field (P-E) curves were measured with a Precision Multiferroic II Ferroelectric Test System (Radiant Technologies Inc. Albuquerque NM) under AC electric fields at 100 Hz. Switching current loops were measured under AC electric fields at 50 Hz with the same tool. Dielectric permittivity as a function of DC electric field was measured by an aixACCT DBLI system (aixACCT Systems

GmbH, Germany) with a small signal voltage of 2 V and 1 kHz frequency. The DBLI tool was also used for evaluation of effective piezoelectric coefficients under a small signal voltage of 2 V at 1 kHz. Strain curves were also measured by the DBLI tool under AC electric fields at 100 Hz frequency averaged over 200 cycles. AC electric field dependent relative dielectric permittivity was also evaluated in the DBLI system under a superimposed DC voltage of 3 V and increasing AC voltages with step size of 0.1 V and frequency of 1 kHz. The dielectric and electromechanical properties of the samples remain mostly invariant after the full set of measurements.

Supporting Information Supporting Information is available from the Wiley Online Library or from the author.

Acknowledgements

N.B.-G. and Y.Y. acknowledge financial support by the U.S. National Science Foundation under grant No. CMMI-1537262, DMR- 2026976. N.B.-G. and Z.B. also acknowledge financial support by the U.S. National Science Foundation under grant DMR-2219476 and the Harris Saunders Jr. Chair endowment at Georgia Tech. A.B.N. acknowledges financial support by the Engineering and Physical Sciences Research Council under grant numbers EP/L017008/1, EP/R023751/1 and EP/T019298/1. S.L. and I.P. acknowledge financial support by the U.S. Department of Energy, Office of Basic Energy Sciences, Division of Materials Sciences and Engineering under grant DE-SC0005245. A.K. gratefully acknowledges support by Department of Education and Learning, Northern Ireland through the US-Ireland R&D partnership Grant No. USI-211.

References

[1] X. Hao, J. Zhai, L. B. Kong, Z. Xu, *Progress in Materials Science* **2014**, *63* 1.

[2] X. Hao, *Journal of Advanced Dielectrics* **2013**, *03*, 01 1330001.

[3] C. Kittel, *Physical Review* **1951**, *82*, 5 729.

[4] E. Sawaguchi, H. Maniwa, S. Hoshino, *Physical Review* **1951**, *83*, 5 1078.

[5] M. Gao, X. Tang, S. Dai, J. Li, D. Viehland, *Applied Physics Letters* **2019**, *115*, 7 072901.

[6] Z. Fu, X. Chen, Z. Li, T. Hu, L. Zhang, P. Lu, S. Zhang, G. Wang, X. Dong, F. Xu, *Nature Communications* **2020**, *11*, 1 3809.

[7] C. Milesi-Brault, N. Godard, S. Girod, Y. Fleming, B. El Adib, N. Valle, S. Glinšek, E. Defay, M. Guennou, *Applied Physics Letters* **2021**, *118*, 4 042901.

[8] X.-K. Wei, C.-L. Jia, H.-C. Du, K. Roleder, J. Mayer, R. E. Dunin-Borkowski, *Advanced Materials* **2020**, *32*, 9 1907208.

[9] J. S. Baker, M. Pa'sciak, J. K. Shenton, P. Vale" Castro, B. Xu, J. Hlinka, P. M'arton, R. G. Burkovsky, G. Catalán, A. M. Glazer, D. R. Bowler, A re-examination of antiferroelectric pbzro3 and pbhfo3: an 80-atom pnam structure, **2021**.

[10] H. Aramberri, C. Cazorla, M. Stengel, J. Íñiguez, *npj Computational Materials* **2021**, *7*, 1 196.

[11] A. Roy Chaudhuri, M. Arredondo, A. Hähnel, A. Morelli, M. Becker, M. Alexe, I. Vrejoiu, *Physical Review B* **2011**, *84* 054112.

[12] B. K. Mani, R. Herchig, E. Glazkova, S. Lisenkov, I. Ponomareva, *Nanotechnology* **2016**, *27*, 19 195705.

[13] P. Ayyub, S. Chattopadhyay, R. Pinto, M. Multani, *Physical Review B* **1998**, *57* R5559.

[14] L. Pintilie, K. Boldyreva, M. Alexe, D. Hesse, *Journal of Applied Physics* **2008**, *103* 024101.

[15] F. K. Lotgering, *Journal of Inorganic and Nuclear Chemistry* **1959**, *9*, 2 113.

[16] F. Jona, G. Shirane, F. Mazzi, R. Pepinsky, *Physical Review* **1957**, *105*, 3 849.

[17] N. Bassiri-Gharb, I. Fujii, E. Hong, S. Trolier-McKinstry, D. Taylor, D. Damjanovic, *Journal of Electroceramics* **2007**, *19* 49.

[18] X. Dai, J.-F. Li, D. Viehland, *Physical Review B* **1995**, *51*, 5 2651.

[19] S. Teslic, T. Egami, *Acta Crystallographica Section B* **1998**, *54*, 6 750.

[20] R. Gao, S. E. Reyes-Lillo, R. Xu, A. Dasgupta, Y. Dong, L. R. Dedon, J. Kim, S. Saremi, Z. Chen, C. R. Serrao, H. Zhou, J. B. Neaton, L. W. Martin, *Chemistry of Materials* **2017**, *29*, 15 6544.

[21] O. E. Fesenko, V. G. Smotrakov, *Ferroelectrics* **1976**, *12*, 1 211.

[22] O. E. Fesenko, R. V. Kolesova, Y. G. Sindeyev, *Ferroelectrics* **1978**, *20*, 1 177.

[23] B. K. Mani, S. Lisenkov, I. Ponomareva, *Physical Review B* **2015**, *91*, 13 134112.

[24] A. K. Tagantsev, K. Vaideeswaran, S. B. Vakhrushev, A. V. Filimonov, R. G. Burkovsky, A. Shaganov, D. Andronikova, A. I. Rudskoy, A. Q. R. Baron, H. Uchiyama, D. Chernyshov, A. Bosak, Z. Ujma, K. Roleder, A. Majchrowski, J. H. Ko, N. Setter, *Nature Communications* **2013**, *4*, 1 2229.

[25] S. E. Reyes-Lillo, K. M. Rabe, *Physical Review B* **2013**, *88*, 18 180102.

[26] Z. Fan, T. Ma, J. Wei, T. Q. Yang, L. Zhou, X. Tan, *Journal of Materials Science* **2020**, *55* 4953 .

[27] Z. Xu, D. Viehland, D. A. Payne, *Proceedings of 1994 IEEE International Symposium on Applications of Ferroelectrics* **1994**, 589–590.

[28] R. Blinc, *Ferroelectrics* **1987**, *74*, 1 301.

[29] C. F. Pulvari, *Physical Review* **1960**, *120*, 5 1670.

[30] K. Du, L. Guo, J. Peng, X. Chen, Z.-N. Zhou, Y. Zhang, T. Zheng, Y.-P. Liang, J. Lu, Z.-H. Ni, S.-S. Wang, G. Tendeloo, Z. Zhang, S. Dong, H. Tian, *npj Quantum Materials* **2020**, *5* 49.

[31] S. I. Shkuratov, J. Baird, V. G. Antipov, E. F. Talantsev, H. R. Jo, J. C. Valadez, C. S. Lynch, *Applied Physics Letters* **2014**, *104*, 21 212901.

[32] D. Fang, C. Li, *Journal of Materials Science* **1999**, *34*, 16 4001.

[33] M. Sharifzadeh Mirshekarloo, K. Yao, T. Sritharan, *Applied Physics Letters* **2010**, *97*, 14 142902.

[34] B. Xu, N. G. Pai, Q.-M. Wang, L. E. Cross, *Integrated Ferroelectrics* **1998**, *22*, 1-4 545.

[35] M. D. Nguyen, G. Rijnders, *Thin Solid Films* **2020**, *697* 137843.

[36] A. Davydok, T. W. Cornelius, C. Mocuta, E. C. Lima, E. B. Araujo, O. Thomas, *Thin Solid Films* **2016**, *603* 29.

[37] L. Lian, N. R. Sottos, *Journal of Applied Physics* **2003**, *95*, 2 629.

[38] L. Lian, N. R. Sottos, *Journal of Applied Physics* **2000**, *87*, 8 3941.

[39] Y. Bastani, N. Bassiri-Gharb, *Acta Materialia* **2012**, *60*, 3 1346.

[40] Y. Bastani, T. Schmitz-Kempen, A. Roelofs, N. Bassiri-Gharb, *Journal of Applied Physics* **2011**, *109*, 1 014115.

[41] S.-H. Kim, J.-S. Yang, C. Y. Koo, J.-H. Yeom, E. Yoon, C. S. Hwang, J.-S. Park, S.-G. Kang, D.-J. Kim, J. Ha, *Japanese Journal of Applied Physics* **2003**, *42*, Part 1, No. 9B 5952.

[42] A. L. Kholkin, E. K. Akdogan, A. Safari, P. F. Chauvy, N. Setter, *Journal of Applied Physics* **2001**, *89*, 12 8066.

[43] N. J. Donnelly, G. Catalan, C. Morros, R. M. Bowman, J. M. Gregg, *Journal of Applied Physics* **2003**, *93*, 12 9924.

[44] J. Wang, K. H. Wong, H. L. W. Chan, C. L. Choy, *Applied Physics A* **2004**, *79*, 3 551.

[45] N. Ledermann, P. Muralt, J. Baborowski, S. Gentil, K. Mukati, M. Cantoni, A. Seifert, N. Setter, *Sensors and Actuators A: Physical* **2003**, *105*, 2 162.

[46] Y. Yao, A. B. Naden, F. Zhang, D. Edwards, P. Joshi, B. J. Rodriguez, A. Kumar, N. Bassiri-Gharb, *Journal of the European Ceramic Society* **2020**, *40*, 15 5369.

[47] C. Ophus, J. Ciston, C. T. Nelson, *Ultramicroscopy* **2016**, *162* 1.

[48] M. Nord, P. E. Vullum, I. MacLaren, T. Tybell, R. Holmestad, *Advanced Structural and Chemical Imaging* **2017**, *3*, 1 9.

[49] S. Gates-Rector, T. Blanton, *Powder Diffraction* **2019**, *34*, 4 352.

Table of Contents

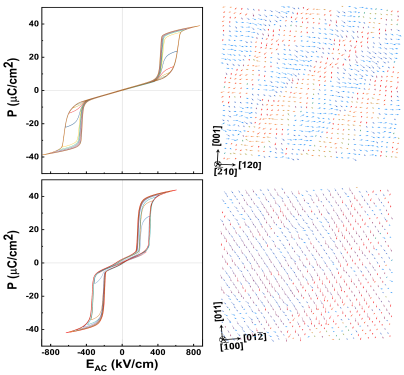

Leveraging highly oriented thin films, a ferrielectric phase is observed in $PbZrO_3$ at room temperature and low field. Ferrielectricity is observed in modulations of amplitude and direction of the spontaneous polarization and large anisotropy for critical electric fields, and is qualitatively consistent with theoretical predictions, and correlates with high dielectric tunability and large strains.